Journal of Solid State Chemistry 182 (2009) 1929–1934

Contents lists available at ScienceDirect

Journal of Solid State Chemistry

journal homepage: www.elsevier.com/locate/jssc

Synthesis, characterization and magnetic property of a new 3D iron phosphite: $|C_4N_3H_{14}|[Fe_3(HPO_3)_4F_2(H_2O)_2]$ with intersecting channels

Jian Qiao, Lirong Zhang, Yang Yu, Guanghua Li, Tianchan Jiang, Qisheng Huo, Yunling Liu *

State Key Laboratory of Inorganic Synthesis and Preparative Chemistry, College of Chemistry, Jilin University, Changchun 130012, PR China

ARTICLE INFO

Article history:
Received 12 February 2009
Received in revised form
28 April 2009
Accepted 3 May 2009
Available online 12 May 2009

Keywords:
Solvothermal synthesis
Crystal structure
Iron phosphite
Mössbauer spectroscopy
Magnetic behavior

ABSTRACT

A new open-framework iron (III) phosphite $|C_4N_3H_{14}|[Fe_3(HPO_3)_4F_2(H_2O)_2]$ has been solvothermally synthesized by using diethylenetriamine (DETA) as the structure-directing agent. Single-crystal X-ray diffraction analysis reveals that the compound crystallizes in the monoclinic space group $C2/c$ having unit cell parameters $a = 12.877(3)$ Å, $b = 12.170(2)$ Å, $c = 12.159(2)$ Å, $\beta = 93.99(3)^\circ$, $V = 1900.9(7)$ Å^3, and $Z = 4$ with $R_1 = 0.0447$, w$R_2 = 0.0958$. The complex structure consists of HPO_3 pseudo-tetrahedra and $\{Fe_3O_{14}F_2\}$ trimer building units. The assembly of these building units generates 3D inorganic framework with intersecting 6-, 8-, and 10-ring channels. The DETA cations are located in the 10-ring channels linked by hydrogen bonds. The Mössbauer spectrum shows that there exhibit two crystallographically independent iron (III) atoms. And the magnetic investigation shows the presence of antiferromagnetic interactions. Further characterization of the title compound was performed using X-ray powder diffraction (XRD), infrared (IR) spectra, thermal gravimetric analyses (TGA), inductively coupled plasma (ICP) and elemental analyses.

1. Introduction

Open-framework metal phosphates have been extensively investigated due to their structural architectures and potential applications in catalysis, separation and adsorption [1,2]. Especially, iron phosphates with one- [3] two- [4–6] and three-dimensional (3D) frameworks [7–10] exhibit a rich structural and compositional diversity. Recently, using pyramidal phosphite groups to substitute tetrahedral phosphate units have resulted in a new class of metal phosphites with great success [11]. And lots of organically templated metal phosphites with extended networks have been synthesized and characterized, such as manganese [12], cobalt [13], zinc [14–17] and vanadium [18]. Although the tenor of preparation of metal phosphite framework has achieved success, only a few iron phosphite compounds exist [19–25]. Such as the two iron phosphites reported by Rojo and coworkers, $|C_4N_2H_{14}|[Fe^{II}_{0.86}Fe^{III}_{1.14}(HPO_3)_{1.39}(HPO_4)_{0.47}(PO_4)_{0.14}F_3]$ [20] with a mixed-valence nature and the presence of both the phosphite and hydrogen–phosphate–phosphate oxoanions, $|C_5H_{18}N_3|[Fe_3(HPO_3)_6]$ [21] with a pillared structure formed by the interpenetration of two subnets. Natarajan and coworkers reported the synthesis of the first one-dimensional (1D) iron phosphite–phosphate $|C_{10}H_8N_2|[Fe^{III}(HPO_3)(H_2PO_4)]$ [24].

During the last few years, our group has worked on the synthesis and structural characterization of metal phosphates and phosphites. In the literature, a large number of gallium- [26], indium- [27] and iron- [28] phosphates; as well as, zinc- [14,15,29] and indium- [30] phosphites have been reported. In order to expand the field of research pertaining to iron phosphite materials with excellent properties, our group has chosen to explore the design and synthesis of novel open architectures by introducing the F^- anion as mineralizer and organic template as part of our design strategy. Herein, we report the synthesis, crystal structure and magnetic properties of a 3D open-framework iron phosphite $|C_4N_3H_{14}|[Fe_3(HPO_3)_4F_2(H_2O)_2]$ by using diethylenetriamine (DETA) as the structure-directing agent, which consists of HPO_3 pseudo-tetrahedra and $\{Fe_3O_{14}F_2\}$ trimer building units, giving rise to a 3D inorganic framework with intersecting 6-, 8-, 10-ring channels.

2. Experimental

2.1. Synthesis

The title compound was synthesized by using mild solvothermal conditions under autogenous pressure. Typically, 0.27 g (1 mmol) $FeCl_3 \cdot 6H_2O$ was dissolved in a mixture of 6 mL H_2O and 3 mL ethanol with stirring, followed by addition of 0.44 mL (4 mmol) DETA and 0.41 g (5 mmol) H_3PO_3. HF (48%) was added dropwise to the above reaction mixture. After stirring for 30 min,

* Corresponding author. Fax: +86 431 85168624.
E-mail address: yunling@jlu.edu.cn (Y. Liu).

0022-4596/$ - see front matter © 2009 Elsevier Inc. All rights reserved.
doi:10.1016/j.jssc.2009.05.008

as the final reaction mixture was transferred into a sealed Teflon-lined steel autoclave and heated at 160 °C for 7 days, then slowly cooled to room temperature. The pH of the mixture did not show any appreciable change during the solvothermal reaction and remained at approximately 1.5. The resulting product, light pink stick-like single crystals were separated by filtering, washed with water and acetone, and dried in air. The yield of the reaction was approximately 60% based on iron content.

2.2. Physical methods

The X-ray powder diffraction (XRD) data were collected on a Rigaku/max-2550 diffractometer with Cu$K\alpha$ radiation ($\lambda = 1.5418$ Å, in the 2θ range 4–40°). The elemental analyses were performed on a Perkin-Elmer 2400 element analyzer. The inductively coupled plasma (ICP) analyses were carried out on a Perkin-Elmer Optima 3300DV ICP instrument. The infrared (IR) spectra were recorded within the 400–4000 cm^{-1} region on a Nicolet Impact 410 FTIR spectrometer using KBr pellets. The thermal gravimetric analyses (TGA) were performed on NETZSCH STA449C thermogravimetric analyzer in air with a heating rate of 10 °C min^{-1}. Mössbauer measurements were made on an Oxford MS-500 instrument at room temperature. The radiation source is ^{57}Fe/Pd. The velocity of isomer shifts is calibrated by an α-Fe foil. The temperature variation of the magnetic susceptibility studies have been carried out on powdered sample in the range 4–300 K with an SQUID magnetometer (Quantum Design MPMS-XL SQUID). Measurements were carried out when the sample had been taken through a zero-field-cooled procedure.

2.3. Structural determination

A suitable single crystal with dimensions of $0.34 \times 0.29 \times 0.27$ mm^3 was selected for single-crystal X-ray diffraction analysis. The intensity data were collected on a Rigaku RAXIS-RAPID IP diffractometer, using graphite-monochromated Mo-$K\alpha$ radiation ($\lambda = 0.71073$ Å). The numbers of collected reflections and independent reflections were 9236 and 2163 for $|C_4N_3H_{14}|[Fe_3(HPO_3)_4F_2(H_2O)_2]$. Data processing was accomplished with the SAINT processing program. The structure was solved by direct methods and refined by full-matrix least-squares on F^2 using SHELXTL Version 5.1 [31]. All the iron and phosphorus atoms were first located, then non-hydrogen atoms (C, N and O) were subsequently found in different Fourier maps. The hydrogen atoms of the amine molecule were placed geometrically. All non-hydrogen atoms were refined anisotropically. Crystal data and refinement parameters for the structure determination are presented in Table 1. The final atomic coordinates and the selected bond distances and angles are given in Tables 2 and 3, respectively.

Table 1
Crystal data and structure refinement for $|C_4N_3H_{14}|[Fe_3(HPO_3)_4F_2(H_2O)_2]$.

Empirical formula	$C_4H_{22}F_2Fe_3N_3O_{14}P_4$
Formula weight	665.68
Temperature	298(2) K
Wavelength	0.71073 Å
Crystal system, space group	Monoclinic, $C2/c$
Unit cell dimensions	$a = 12.877(3)$ Å, $\alpha = 90°$ $b = 12.170(2)$ Å, $\beta = 93.99(3)°$ $c = 12.159(2)$ Å, $\gamma = 90°$
Volume	1900.9(7) $Å^3$
Z, Calculated density	4, 2.326 mg/m^3
Absorption coefficient	2.691 mm^{-1}
$F(000)$	1340
Crystal size	$0.34 \times 0.29 \times 0.27$ mm
Theta range for data collection	3.17–27.47°
Limiting indices	$-16 \le h \le 16$, $-15 \le k \le 15$, $-13 \le l \le 15$
Reflections collected/unique	9236/2163 [R(int) = 0.0629]
Completeness to theta = 27.47	99.4%
Refinement method	Full-matrix least-squares on F^2
Data/restraints/parameters	2163/6/159
Goodness-of-fit on F^2	1.107
Final R indices [$I > 2\sigma$ (I)]	$R_1 = 0.0447$, w$R_2 = 0.0958$
R indices (all data)	$R_1 = 0.0661$, w$R_2 = 0.1122$
Largest diff. peak and hole	0.839 and −0.773 e$Å^3$

Table 2
Atomic coordinates ($\times 10^4$) and equivalent isotropic displacement parameters ($Å^2 \times 10^3$) for $|C_4N_3H_{14}|[Fe_3(HPO_3)_4F_2(H_2O)_2]$.

Atom	x	y	z	U^a (eq)
Fe(1)	2489(1)	407(1)	2027(1)	15(1)
Fe(2)	0	−884(1)	2500	15(1)
P(1)	2024(1)	−2246(1)	1763(1)	17(1)
P(2)	1751(1)	211(1)	−559(1)	16(1)
F(1)	938(2)	284(2)	2020(2)	19(1)
O(1)	2647(3)	−1195(3)	1660(3)	26(1)
O(2)	2262(3)	819(3)	430(3)	19(1)
O(3)	2470(3)	2012(3)	2350(3)	25(1)
O(4)	2559(3)	59(3)	3627(3)	29(1)
O(5)	3963(2)	448(3)	1984(3)	17(1)
O(6)	877(3)	−2033(3)	1888(3)	25(1)
O(7)	−824(3)	−867(3)	1056(3)	23(1)
N(1)	4280(4)	1911(4)	407(4)	37(1)
N(2)	5000	1487(6)	−2500	29(2)
C(1)	4769(5)	1378(5)	−528(5)	33(1)
C(2)	4838(5)	2132(5)	−1500(5)	30(1)

[a] U (eq) is defined as one-third of the trace of the orthogonalized U_{ij} tensor.

3. Results and discussion

3.1. Characterization of $|C_4N_3H_{14}|[Fe_3(HPO_3)_4F_2(H_2O)_2]$

As seen in Fig. 1, the powder X-ray diffraction pattern of the title compound is in good agreement with the one simulated based on the data of the single-crystal structure, indicating the purity of the as-synthesized product. The differences in reflection intensity are probably due to preferred orientations in the powder sample.

The results of elemental analysis are consistent with the theoretical values calculated by the single-crystal structural analysis. Analysis found (wt%): Fe, 25.68; P, 18.98; C, 16.65; H, 3.71; N, 9.93. Calcd. (wt%): Fe, 26.61; P, 19.68; C, 16.76; H, 3.67; N, 9.77. The F^- content was determined using a fluoride ion-selective electrode. Found F (wt%): 5.17. Calcd. (wt%): 5.71.

The IR spectrum of the title compound (see Supporting Information Fig. S1) is assigned as follows: the bands at 3251 and 3122 cm^{-1} are attributed to H-bonded, N–H and C–H groups. The band at 2390 cm^{-1} is associated with the typical stretching vibration of terminal P–H bond in phosphite groups. The bands in the region 1330–1592 cm^{-1} are characteristic of diethylenetriamine molecules. The bands at 1087 and 1015 cm^{-1} are associated with the asymmetric and symmetric stretching vibrations of P–O units, and the band at 586 cm^{-1} is related to the bending vibration of P–O bonds.

The TG curve of the title compound (as shown in Supporting Information Fig. S2) shows a major weight loss of 26.6 wt% (calcd. 26.7 wt%) in the temperature range of 200–600 °C. These mass losses can be corresponded to the loss of organic amine (calcd. 15.6 wt%), water (calcd. 5.4 wt%), the HF molecules (calcd. 5.7 wt%) and the oxidation of phosphite–phosphate groups. XRD studies indicated that the final product, upon calcination above 800 °C, is a dense iron phosphate $FePO_4$ (JCPDS: 31-0647).

Table 3
Selected bond lengths (Å) and bond angles (°) for $|C_4N_3H_{14}|[Fe_3(HPO_3)_4F_2(H_2O)_2]$.

Fe(1)–O(5)	1.902(3)	Fe(2)–O(7)#1	1.987(3)
Fe(1)–O(4)	1.986(4)	P(1)–O(6)	1.517(4)
Fe(1)–O(3)	1.994(4)	P(1)–H(1)	1.40(8)
Fe(1)–F(1)	2.003(3)	P(1)–O(1)	1.520(4)
Fe(1)–O(2)	2.008(3)	P(2)–O(4)#3	1.522(4)
Fe(1)–O(1)	2.013(4)	P(2)–O(7)#4	1.526(3)
Fe(2)–O(6)	1.975(4)	P(2)–H(2)	1.34(9)
Fe(2)–O(6)#1	1.975(4)	N(1)–C(1)	1.486(7)
Fe(2)–F(1)	1.979(3)	N(2)–C(2)#7	1.475(6)
Fe(2)–F(1)#1	1.979(3)	O(4–)P(2)#6	1.522(4)
Fe(2)–O(7)	1.987(3)	O(3)–P(1)#5	1.517(3)
O(5)–Fe(1)–O(4)	93.15(15)	O(6)–Fe(2)–F(1)	91.17(13)
O(5)–Fe(1)–O(3)	90.31(15)	O(6)#1–Fe(2)–F(1)	174.90(13)
O(4)–Fe(1)–O(3)	90.93(16)	O(6)–Fe(2)–F(1)#1	174.90(13)
O(5)–Fe(1)–F(1)	176.68(14)	O(6)#1–Fe(2)–F(1)#1	91.17(13)
O(4)–Fe(1)–F(1)	88.03(14)	F(1)–Fe(2)–F(1)#1	88.19(16)
O(3)–Fe(1)–F(1)	92.77(13)	O(6)–Fe(2)–O(7)#1	93.22(16)
O(5)–Fe(1)–O(2)	92.62(14)	O(6)#1–Fe(2)–O(7)#1	87.64(15)
O(4)–Fe(1)–O(2)	173.77(15)	F(1)–Fe(2)–O(7)#1	87.33(13)
O(3)–Fe(1)–O(2)	86.69(15)	F(1)#1–Fe(2)–O(7)#1	91.81(14)
F(1)–Fe(1)–O(2)	86.34(13)	O(6)–Fe(2)–O(7)	87.64(15)
O(5)–Fe(1)–O(1)	84.46(15)	O(6)#1–Fe(2)–O(7)	93.22(16)
O(4)–Fe(1)–O(1)	90.73(16)	F(1)–Fe(2)–O(7)	91.81(14)
O(3)–Fe(1)–O(1)	174.59(15)	F(1)#1–Fe(2)–O(7)	87.33(13)
F(1)–Fe(1)–O(1)	92.43(13)	O(7)#1–Fe(2)–O(7)	178.8(2)
O(2)–Fe(1)–O(1)	92.16(15)	Fe(2)–F(1)–Fe(1)	132.96(14)
O(6)–P(1)–O(3)#2	113.8(2)	P(1)–O(1)–Fe(1)	137.3(2)
O(6)–P(1)–O(1)	112.8(2)	P(2)–O(2)–Fe(1)	132.0(2)
O(3)#2–P(1)–O(1)	110.9(2)	P(1)#5–O(3)–Fe(1)	135.4(2)
O(4)#3–P(2)–O(2)	110.0(2)	P(2)#6–O(4)–Fe(1)	134.1(2)
O(4)#3–P(2)–O(7)#4	114.0(2)	C(2)-N(2)–C(2)#7	115.5(6)
O(2)–P(2)–O(7)#4	110.0(2)	N(1)–C(1)–C(2)	112.7(5)
P(1)–O(6)–Fe(2)	138.1(2)	N(2)–C(2)–C(1)	110.0(5)
O(6)–Fe(2)–O(6)#1	89.9(2)	P(2)#4–O(7)–Fe(2)	135.3(2)

Symmetry transformations used to generate equivalent atoms: #1 $-x, y, -z+\frac{1}{2}$ #2 $x, -y, z-\frac{1}{2}$ #3 $-x, -y, -z$ #4 $-x+\frac{1}{2}, y-\frac{1}{2}, -z+\frac{1}{2}$ #5 $x, -y, z+\frac{1}{2}$ #6 $-x+\frac{1}{2}, y+\frac{1}{2}, -z+\frac{1}{2}$ #7 $-x+1, y, -z-\frac{1}{2}$.

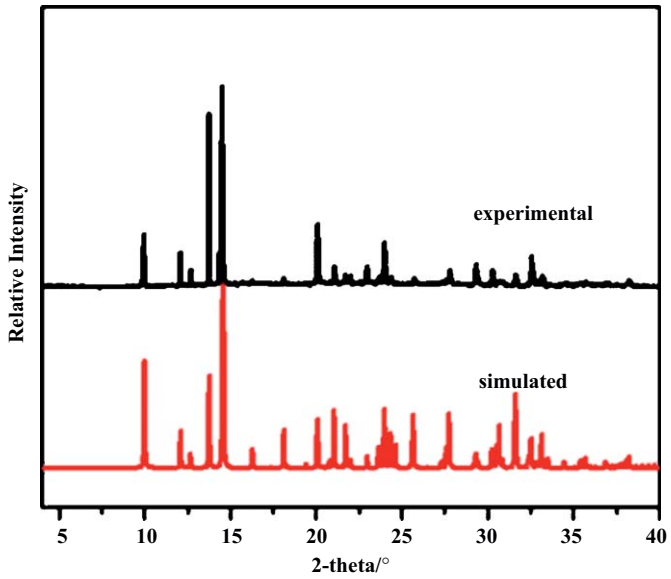

Fig. 1. Simulated and experimental X-ray powder diffraction patterns of $|C_4N_3H_{14}|[Fe_3(HPO_3)_4F_2(H_2O)_2]$.

3.2. Crystal structure of $|C_4N_3H_{14}|[Fe_3(HPO_3)_4F_2(H_2O)_2]$

Single-crystal X-ray diffraction analysis indicates that the compound crystallizes in the monoclinic space group *C*2/*c* with the formula of $|C_4N_3H_{14}|[Fe_3(HPO_3)_4F_2(H_2O)_2]$. As seen in Fig. 2, each asymmetric unit contains 25 non-hydrogen atoms, including two crystallographically distinct Fe atoms and two distinct P atoms. Fe(1) atom shares five oxygen atoms and one fluorine atom to form $Fe(1)O_5F$ octahedron [Fe(1)–O bond lengths in the range of 1.903(3)–2.013(4) Å, Fe(1)–F bond length of 2.003(3) Å]. Fe(2) atom shares four oxygen atoms and two fluorine atoms to form $Fe(2)O_4F_2$ octahedron [Fe(2)–O bond lengths in the range of 1.975(4)–1.987(3) Å, Fe(2)–F bond length of 1.979(3) Å]. The O–Fe–O bond angles are in the range of 84.46(15)–178.8(2)°, O–Fe–F bond angles are in the range of 86.34–176.67(14)°. Both of P(1) and P(2) atoms link to two Fe(1) and one Fe(2) atoms via three bridging oxygen atoms and one H atom (P–O average bond distance: 1.52 Å, P–H average bond distance: 1.37 Å). The O–P–O bond angles are in the range of 110.0(2)–114.0(2)°.

The $|C_4N_3H_{14}|[Fe_3(HPO_3)_4F_2(H_2O)_2]$ compound exhibits a 3D open-framework formed by the unusual $\{Fe_3O_{14}F_2\}$ trimer units. Two $\{FeO_5F\}$ octahedra and a $\{FeO_4F_2\}$ octahedron linked by two bridging F atoms formed the trimer units, further linked by four $\{HPO_3\}$ groups to generate the unique $\{Fe_3P_4O_{18}F_2\}$ building blocks (see Fig. 3). This kind of building blocks based on vertex sharing O atoms form an interesting layer with the 10-ring windows along the [001] direction (see Fig. 4). These layers further connect with each other by $HP(2)O_3$ pyramidal tetrahedron, which constructed the 6-ring channels in *ac* plane (see Supporting Information Fig. S5), generate the 3D open-framework. Furthermore, this kind of trimer unit in $|C_4N_3H_{14}|[Fe_3(HPO_3)_4F_2(H_2O)_2]$ is similar to the secondary building unit of $\{M_3O_{20}T_4\}$ [11] found in iron phosphate or phosphite materials. The difference is two F atoms instead of O atoms serve as bridging atoms with the connection of Fe–F–Fe–F–Fe in the $\{Fe_3P_4O_{18}F_2\}$ unit of the title compound. The structure of the title compound also can be described on the base of 8-rings 2D sheets parallel to the *bc* plane, which is perpendicular to the 10-ring layers (as shown in Fig. 5). These layers were further connected with each other by $Fe(2)O_4F_2$ octahedron to generate the 3D open-framework. Fig. 6 shows the H-bondings arrangement between the DETA cations and the host framework. Each guest molecular forms seven hydrogen bondings to the bridging and oxygen atoms in the structure. The N⋯O distances are in the range of 2.670(7)–3.150(4) Å.

It is of interesting that the compound possesses intersecting channels with 6-, 8- and 10-ring pore openings. The 10-ring channel along the *c*-axis possesses an aperture of approximately 6.3 × 11.0 Å (O–O distance). The 8-ring channel perpendicular to 10-ring channels is 5.3 × 6.8 Å and the 6-ring channel along *b*-axis is 4.7 × 5.8 Å with a pore diameter (as shown in Figs. S4 and S5, see Supporting Information). These channels are intersecting with each other, and the DETA cations reside in the "free" space of the intersecting channels. Two DETA are occluded in one 10-ring pore (as shown in Fig. S6). They arrange in a manner that the end of one template cation exclusively protrudes to the other one, while the hydrophilic amino groups closely interact with the charged inorganic framework through weak H-bonds: N(1)–H(1B)⋯O(7): 2.822(6), N(1)–H(1B)⋯O(6): 2.934(6), N(2)–H(2A)⋯O(5): 2.758(7) Å. The similar behavior has been found in other zincophosphite [17], which exhibit intersecting 8-, 12-, and 16-ring channels. Comparing to the coordination number (CN) of zinc is four, the CN of iron(III) is six, it is easier for HPO_3 units to connect to four-coordinate zinc to form a larger pore than the usually six-coordinate transition-metal elements [11,32].

3.3. Mössbauer spectroscopy

The Mössbauer spectrum of $|C_4N_3H_{14}|[Fe_3(HPO_3)_4F_2(H_2O)_2]$ (Fig. 7) recorded in the paramagnetic state at 300 K shows a signal

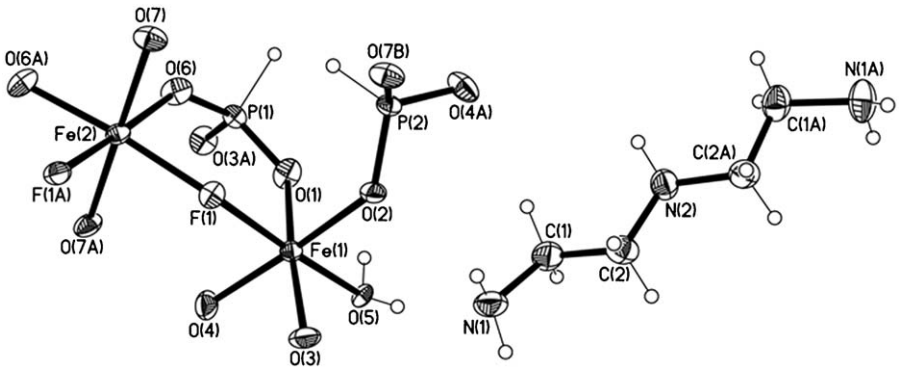

Fig. 2. ORTEP view of the asymmetric unit of $|C_4N_3H_{14}|[Fe_3(HPO_3)_4F_2(H_2O)_2]$ (50% thermal ellipsoids).

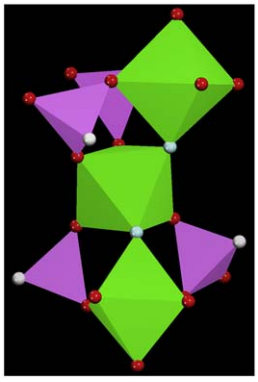

Fig. 3. The $\{Fe_3P_4O_{18}F_2\}$ building block of $|C_4N_3H_{14}|[Fe_3(HPO_3)_4F_2(H_2O)_2]$. Color code: Fe: green; P: pink. (For interpretation of the references to the color in this figure legend, the reader is referred to the web version of this article.)

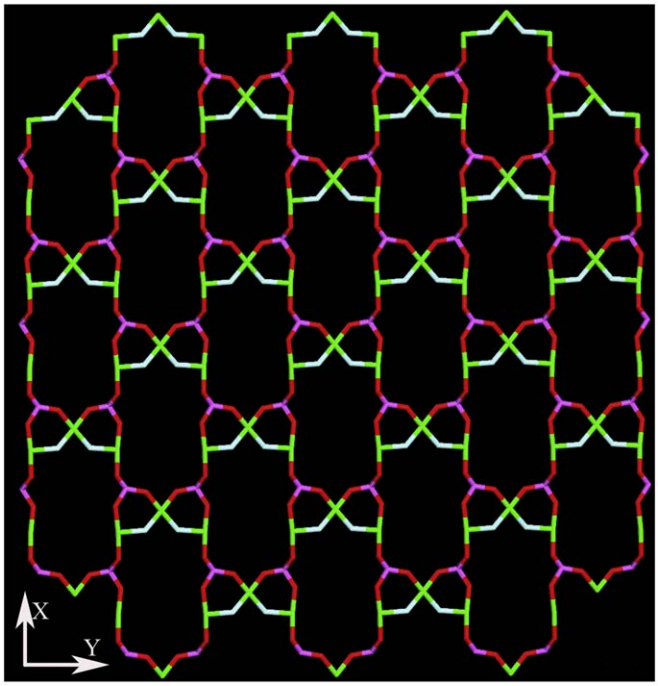

Fig. 4. The 10-ring sheet of $|C_4N_3H_{14}|[Fe_3(HPO_3)_4F_2(H_2O)_2]$ parallel to *ab* plane, which consists of four $\{Fe_3P_4O_{18}F_2\}$ building blocks connect via HPO_3 pyramidal tetrahedron, all H atom and coordinated water are omitted for clarity are omitted for clarity.

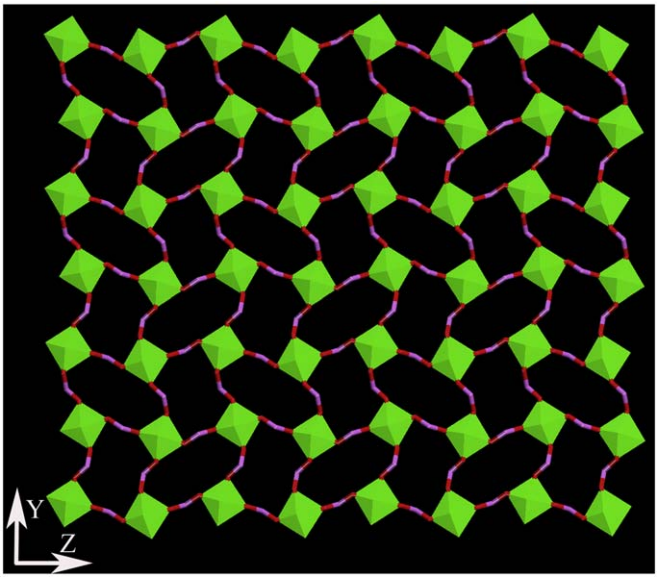

Fig. 5. The 8-ring layer along [100] direction, which perpendicular to 10-ring layers, all H atoms are omitted for clarity are omitted for clarity.

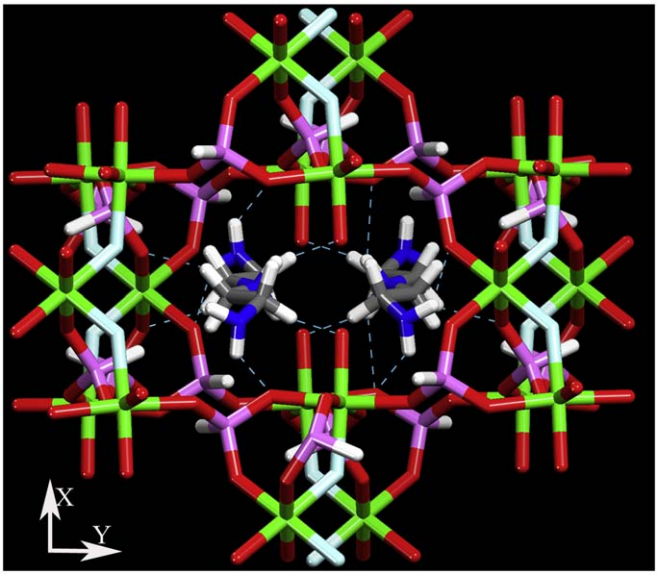

Fig. 6. H-bonding arrangement between the DETA cations and the host framework.

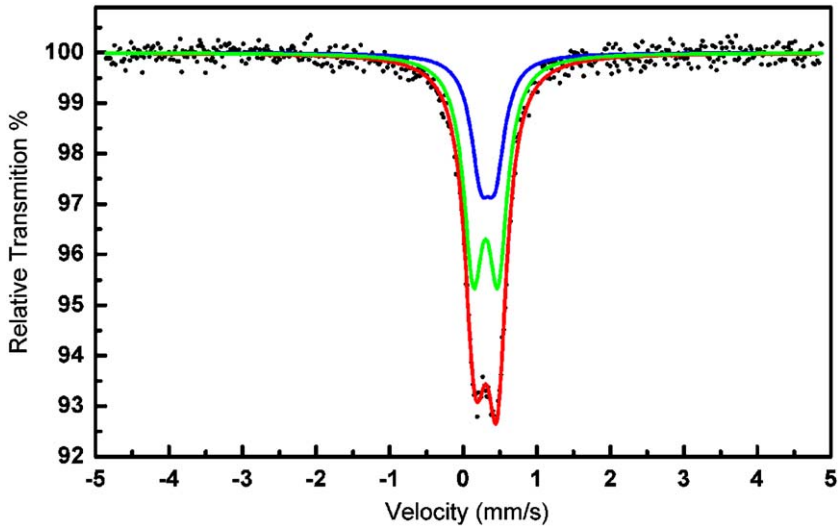

Fig. 7. Mössbauer spectrum of $|C_4N_3H_{14}|[Fe_3(HPO_3)_4F_2(H_2O)_2]$. Color code: Fe(1): green; Fe(2): blue. (For interpretation of the references to the color in this figure legend, the reader is referred to the web version of this article.)

Table 4
Isomer shift (IS) relative to α-Fe metal, quadrupole splitting (QS), the value of width at half-maximum (WHM) and relative spectral areas (RSA) of ^{57}Fe/Pd Mössbauer spectrum $|C_4N_3H_{14}|[Fe_3(HPO_3)_4F_2(H_2O)_2]$ at 300 K.

Site	IS (mm/s)	QS (mm/s)	WHM (mm/s)	RSA (%)
Fe(1)	0.42	0.34	0.32	66.2
Fe(2)	0.45	0.20	0.32	33.8

composed of two symmetric doublets corresponding to the iron cations. The values obtained for the isomer shift and the quadrupole splitting characterizes iron(III) ions in highly symmetric octahedral coordination (Table 4) [21,28]. In 2001, Lazoryak and coworkers reported an iron phosphate $Na_3Fe(PO_4)_2$, with the value of width at half-maximum (WHM) of iron(III) is 0.31 mm s^{-1} [33]. In 2006, Pilawa and coworkers reported a cyclic spin-cluster $Fe_6(tea)_6(CH_3OH)_6$ with the WHM of iron (III) is 0.365 mm s^{-1} [34]. Comparing the 0.32 mm s^{-1} WHM of the title compound with this two compounds, it proves that Fe^{3+} ions in the title compound are in an octahedral environment and are typical of high-spin Fe^{3+} ions. The relative spectral areas are approximately in the 2:1 ratio of the Fe(1) and Fe(2) cations, respectively. This result confirms the existence of non-equivalent positions for the iron(III) cations obtained from single-crystal X-ray structural refinement.

3.4. Magnetic properties

Magnetic measurement was performed on powdered sample from room temperature to 4 K (as shown in Supporting Information Fig. S3). While temperature higher than 90 K, the magnetic behavior can be fitted by the Curie–Weiss law, as shown in $1/\chi_m$–T pattern, and gives values $C_m = 13.07$ cm^3 K mol^{-1} and $\theta = -143.87$ K. An effective magnetic moment of 5.90μ_B for the free Fe (III) ion was calculated by formula $\mu_{eff} = (8C_m)^{1/2}$. The calculated value was agreed well to the theory value of the high-spin Fe^{3+} ion [35]. The negative Weiss temperature and continuous decrease of the $\chi_m T$ product from 8.87 cm^3 K mol^{-1} at room temperature down to 0.85 cm^3 K mol^{-1} at 4 K indicate the existence of antiferromagnetic interactions.

4. Conclusion

In this paper, we have successfully solvothermally synthesized a novel iron phosphite, $|C_4N_3H_{14}|[Fe_3(HPO_3)_4F_2(H_2O)_2]$, by using DETA as organic structure-directing agent. The title compound exhibits a novel 3D structure with intersecting 6-, 8-, 10-ring channels. The Mössbauer spectrum shows that there exhibit two crystallographically independent iron (III) atoms. And the magnetic investigations show the presence of canted-antiferromagnetic interactions. It is believed that iron phosphites with more novel structures will be synthesized by the variation of the organic amines and crystallization conditions.

Supporting information and structure details

Crystallographic data for the structure reported in this paper in the form of CIF file have been deposited with the Cambridge Crystallographic Data Centre as supplementary publication no. CCDC- 710531 for $|C_4N_3H_{14}|[Fe_3(HPO_3)_4F_2(H_2O)_2]$. Copies of the data can be obtained free of charge on application to CCDC, 12 Union Road, Cambridge CB2 1EZ, UK (Fax: +44 1223 336 033; E-mail: deposit@ccdc.cam.ac.uk).

Acknowledgments

The authors acknowledge the financial support of the Natural Science Foundation of China (Grant nos. 20671041 and 20701015) and the State Key Laboratory of Inorganic Synthesis and Preparative Chemistry of Jilin University.

Appendix A. Supplementary material

Supplementary data associated with this article can be found in the online version at doi:10.1016/j.jssc.2009.05.008.

References

[1] C.N.R. Rao, S. Natarajan, A. Choudhury, S. Neeraj, A.A. Ayi, Acc. Chem. Res. 34 (2001) 80 and references therein.

[2] R. Murugavel, A. Choudhury, M.G. Walawalkar, R. Pothiraja, C.N.R. Rao, Chem. Rev. 108 (2008) 3549.
[3] I. Macdonald, W.T.A. Harrison, Inorg. Chem. 41 (2002) 6184.
[4] S. Neeraj, S. Natarajan, C.N.R. Rao, Dalton Trans. (2000) 2499.
[5] S. Natarajan, Inorg. Chem. 41 (2002) 5530.
[6] S. Neeraj, S. Natarajan, C.N.R. Rao, Chem. Commun. (1999) 165.
[7] A. Choudhury, S. Natarajan, C.N.R. Rao, Chem. Commun. (1999) 1305.
[8] M. Cavellec, D. Riou, G. Ferey, Inorg. Chim. Acta 291 (1999) 317.
[9] K. Lii, Y. Huang, Chem. Commun. (1997) 839.
[10] J.R.D. DeBord, W.M. Reiff, C.J. Warren, R.C. Haushalter, J. Zubieta, Chem. Mater. 9 (1997) 1994.
[11] S. Natarajan, S. Mandal, Angew. Chem. Int. Ed. 47 (2008) 4798.
[12] S. Fernandez, J.L. Mesa, J.L. Pizarro, L. Lezama, M.I. Arriortua, R. Olazcuaga, T. Rojo, Chem. Mater. 12 (2000) 2092.
[13] S. Fernandez, J.L. Mesa, J.L. Pizarro, L. Lezama, M.I. Arriortua, T. Rojo, Int. J. Inorg. Mater. 3 (2001) 331.
[14] J. Qiao, L.R. Zhang, L. Liu, Y. Yu, M.H. Bi, Q.S. Huo, Y.L. Liu, J. Solid State Chem. 181 (2008) 2908.
[15] L. Liu, Y.L. Liu, G.H. Li, C. Chen, M.H. Bi, W.Q. Pang, J. Solid State Chem. 179 (2005) 1312.
[16] J. Liang, J.Y. Li, J.H. Yu, P. Chen, Q. Fang, F. Sun, R. Xu, Angew. Chem. Int. Ed. 45 (2006) 2546.
[17] J. Liang, J. Li, J. Yu, P. Chen, L. Li, R. Xu, J. Solid State Chem. 179 (2006) 1977.
[18] X.M. Jing, L.R. Zhang, S.Z. Gong, G.H. Li, M.H. Bi, Q.S. Huo, Y.L. Liu, Micropor. Mesoporo. Mater. 116 (2008) 101.
[19] S. Fernandez, J.L. Mesa, J.L. Pizarro, L. Lezama, M.I. Arriortua, T. Rojo, Chem. Mater. 14 (2002) 2300.
[20] S. Fernandez-Armas, J.L. Mesa, J.L. Pizarro, J.S. Garitaonandia, M.I. Arriortua, T. Rojo, Angew. Chem. Int. Ed. 43 (2004) 977.
[21] U. Chuang, J.L. Mesa, J.L. Pizarro, J.R. Fernández, J.S. Marcos, J.S. Garitaonandia, M.I. Arriortua, T. Rojo, Inorg. Chem. 45 (2006) 8965.
[22] S. Fernandez-Armas, J.L. Mesa, J.L. Pizarro, M.I. Arriortua, T. Rojo, Mater. Res. Bull. 42 (2007) 544.
[23] S.F. Armas, J.L. Mesa, J.L. Pizarro, J.M. Clemente-Juan, E. Coronado, M.I. Arriortua, T. Rojo, Inorg. Chem. 45 (2006) 3240.
[24] S. Mandal, S.K. Pati, M.A. Green, S. Natarajan, Chem. Mater. 17 (2005) 638.
[25] S. Mandal, D. Banerjee, S.V. Bhat, S.K. Pati, S. Natarajan, Eur. J. Inorg. Chem. (2008) 1386.
[26] Y. Yang, Y. Liu, Z. Mu, L. Ye, T. Hu, C. Chen, W. Pang, J. Solid State Chem. 177 (2000) 696.
[27] C. Chen, S. Wang, N. Zhang, Z. Yan, W. Pang, Micropor. Mesoporo. Mater. 106 (2007) 1.
[28] H. Meng, G.H. Li, Y.L. Liu, L. Liu, Y.J. Cui, W. Pang, J. Solid State Chem. 177 (2004) 4459.
[29] L. Liu, L. Zhang, X. Wang, G. Li, Y. Liu, W. Pang, Dalton Trans. (2008) 2009.
[30] Z. Yi, C. Chen, S. Li, G. Li, H. Meng, Y. Cui, Y. Yang, W. Pang, Inorg. Chem. Commun. 8 (2005) 166.
[31] G.M. Sheldrick, SHELXTL-NT, Version 5.1, Bruker AXS Inc., Madison, WI, 1997.
[32] W.K. Li, G.D. Zhou, T. Mak, Advanced Inorganic Structural Chemistry, Oxford University Press, Beijing, 2008.
[33] V.A. Morozov, B.I. Lazoryak, A.P. Malakho, K.V. Pokholok, S.N. Polyakov, T.P. Terekhina, J. Solid State Chem. 160 (2001) 377.
[34] J. Kreitlow, J. Litterst, S. Süllow, B. Pilawa, Hyperfine Interact. 168 (2006) 1197.
[35] R. Carlin, Magnetochemistry, Springer, Berlin, Heidelberg, 1986.